Article   https://doi.org/10.1038/s41929-022-00846-8

Hydrogen bond network connectivity in the electric double layer dominates the kinetic pH effect in hydrogen electrocatalysis on Pt

Peng Li[1,3], Yaling Jiang[1,3], Youcheng Hu[1], Yana Men[1], Yuwen Liu[1], Wenbin Cai ⓘ [2] and Shengli Chen ⓘ [1]✉

The origin of the large kinetic pH effect in hydrogen electrocatalysis, that is, the approximately two orders of magnitude decrease in reaction kinetics when moving from acid to alkaline, remains far from having a consensus. Here we show that it is the significantly different connectivity of hydrogen-bond networks in electric double layers that causes the large kinetic pH effect. This result has been obtained by meticulously comparing the electric double layers of acid and alkaline interfaces from ab initio molecular dynamics simulations, and the computed vibrational density of states of water molecules in the interfaces simulated with ab initio molecular dynamics, with the results of in situ surface-enhanced infrared absorption spectroscopy. Using a Pt–Ru alloy as a model catalyst, we further reveal an unanticipated role of OH adsorption in improving the kinetics of alkaline hydrogen electrocatalysis, namely, by increasing the connectivity of hydrogen-bond networks in electric double layers rather than by merely affecting the energetics of surface reaction steps. These findings highlight the key roles of electric double layer structures in electrocatalysis.

Due to its high energy density and carbon-free nature, hydrogen is considered the most promising energy carrier of the future[1,2]. The hydrogen evolution reaction (HER) and hydrogen oxidation reaction (HOR) are the cornerstones of the hydrogen energy approach. Besides their technological importance in water electrolysis and fuel cells, the HER and HOR have long served as the model reactions in electrochemistry due to their relatively simple reaction mechanisms[3,4]. A standing puzzle in the fundamental chemistry of hydrogen electrocatalysis is the origin of the orders of magnitude decrease in reaction kinetics when moving from acid to alkaline, which has seriously retarded the further development of electrochemical energy technologies based on alkaline electrolytes, and therefore has attracted great recent research interest[5–9].

So far, several schools of thought exist to explain the kinetic sluggishness of HER/HOR in alkaline environments. Yan and coworkers attributed it to the pH-dependent hydrogen binding energy (HBE)[10–14].

They found that the apparent HBE values, inferred from the potential of underpotential-deposited hydrogen (H_{upd}) peaks in cyclic voltammetry plots, linearly increase with the pH, while the experimental HER/HOR activity decreases with the pH. On this basis, the HBE has been proposed to be the sole descriptor for the HER/HOR activity. However, it has been argued that the shift of the voltametric peak for H_{upd} is due to the change in the hydroxyl adsorption strength[15,16]. Additionally, the HBE theory cannot explain the pH-dependence of HER/HOR kinetics on a Pt(111) surface, at which the cyclic voltammetry peak for H_{upd} hardly shifts with pH[17]. What's more, the results from in situ surface-enhanced infrared adsorption spectroscopy (SEIRAS) and surface-enhanced Raman spectroscopy have indicated that the H binding strength is weakened as pH increases, thus challenging the foundation of the HBE theory[18,19].

Another prevailing school of thought suggests that the high activation barrier of an alkaline Volmer step ($H_2O + e^- \leftrightarrow {}^*H + OH^-$, where e^- is an electron) derived from the cleavage/formation of a H–OH

[1]College of Chemistry and Molecular Sciences, Wuhan University, Wuhan, China. [2]Department of Chemistry, Fudan University, Shanghai, China. [3]These authors contributed equally: Peng Li, Yaling Jiang. ✉e-mail: slchen@whu.edu.cn

bond is the origin of the pH effect on HER/HOR kinetics[6]. By contrast, having hydronium ions as the proton donors in an acidic environment implies an unobstructed Volmer step ($H_3O^+ + e^- \leftrightarrow$ *H + H_2O). Markovic and coworkers reported that the combination of Pt with components having high oxophilicity, such as hydroxides, oxides, Ru and so on, can distinctly promote the dissociation of water and/or the adsorption of hydroxyl species, thereby enhancing HER/HOR kinetics in an alkaline environment[20–22]. The so-called bi-functional mechanism thus proposed has been widely used nowadays to guide the design of high-efficiency alkaline HER/HOR electrocatalysts[23,24]. However, this view was questioned by some results that imply that the electronic effect of Ru is responsible for the enhanced hydrogen reaction kinetics at high pH[7,25]. Meanwhile, the role of hydroxyl species (OH⁻ or adsorbed OH (OH_{ad})) in alkaline hydrogen electrocatalysis are still elusive and the subject of extensive debate[26–29].

The pH-dependent kinetics of HER/HOR have also been attributed to the variation in interfacial environment with pH. Koper and coworkers contended that the great deviation of electrode potential from the potential of zero charge (PZC) leads to a strong interfacial electrical field, which significantly increases the water-reorganization energy, and thus impedes the proton/hydroxide transfer in the electrical double layer (EDL)[17]. Following this idea, the pH-dependent kinetics on the Pt(111) electrode and the activity improvement of alkaline hydrogen electrocatalytic reactions by introducing $Ni(OH)_2$ on Pt have been explained in terms of interfacial rigidity associated with the PZC. Other EDL factors, such as electrostatic interactions and water dynamics, also have been proposed to contribute to the pH-dependent kinetics of HER/HOR[30,31]. In addition, the solvation of reaction species also can crucially contribute to the reaction free energy at electrified interfaces, as accounted for in a mean-field way by the Marcus theory of electron transfer, which has also been highlighted in recent studies[32–35]. Last but not least, some researchers have recently proposed that the interfacial hydrogen-bond (H-bond) networks may play a critical role in the kinetics of interfacial proton-coupled electron transfer reactions[36–38]. So far, these EDL propositions lack atomic- or molecular-level evidence.

In this study, taking the HER/HOR on Pt as the model system, the underlying origin of the pH-dependent reaction kinetics is investigated by combining ab initio molecular dynamics (AIMD) simulation and in situ SEIRAS with the attenuated total reflection (ATR) configuration. The AIMD simulation results imply that neither the hydrogen adsorption strength nor the water dissociation/formation barrier is responsible for the greatly reduced kinetics of hydrogen electrocatalysis in alkaline solution. Interestingly, by carefully analysing the AIMD-simulated EDL structures, we notice that a visible gap of water exists at the alkaline interface, which should result in greatly reduced connectivity of H-bond networks and therefore an increased hydrogen transfer barrier in the interfacial region. More importantly, the simulated interfacial structures are unequivocally verified by the agreement between the computational vibrational density of states (VDOS) and the experimental SEIRAS results. What's more, the AIMD simulations for a Pt–Ru alloy show that the OH_{ad} on a Ru site can significantly improve the connectivity of H-bond networks at the alkaline interface. This unanticipated role of OH_{ad} explains well why Pt–Ru is much more active than Pt for hydrogen electrocatalytic reactions in alkaline conditions, and further confirms the critical role of interfacial H-bond connectivity in HER/HOR kinetics. These findings should add important insight into the critical role of the interfacial EDL in electrocatalytic kinetics and provide a unique perspective to understand the electrocatalytic pH effects, which are of general significance in various energy conversion reactions such as HER/HOR, CO_2 reduction and nitrogen reduction. Meanwhile, this study also offers a research paradigm for reference, for exploring the structures and processes at electrochemical interfaces by combining AIMD simulations, computational spectroscopy and experimental spectroscopy.

Results

Acid and alkaline EDLs in hydrogen electrocatalysis

For the interface models with a 4 × 4 orthogonal Pt(111) slab used in the present study (Supplementary Figs. 1–3), the introduction of two H_3O^+ or four Na^+ cations into the water layers, and the same number of electrons into the electrode, can drive the electrode potentials (U) to values corresponding to the HER potentials for acid and alkaline systems, that is, approximately −0.20 V for pH = 0 and approximately −0.32 V for pH = 14 (unless stated, potentials in this work are referenced to the reversible hydrogen electrode, RHE). The much higher electron density on the electrode surface for the alkaline system is easy to understand when considering that the HER potentials are much further away from the PZC. As stated in the Methods, the co-ions and the Gouy–Chapman diffusion layer can be neglected in the strong acid and alkaline systems. Therefore, we focus on the differences between the EDL structures at the acid and alkaline interfaces associated with the profiles of cations. Figure 1a,b show the representative AIMD snapshots for the acid and alkaline interfaces, respectively. The statistic concentration profiles and trajectory analyses of H_3O^+ and Na^+ distinctly demonstrate a layered distribution of cation in both acid and alkaline EDLs (Supplementary Fig. 4).

The planes consisting of the cations closest to the electrode surface are defined as the closest ion planes (CIPs), which are at distances of ~4.26 Å and ~2.92 Å away from the electrode surface for acid and alkaline systems, respectively. The alkaline CIP bears a much higher ion concentration than the acid one. The crowded cations at the alkaline CIP lose considerably their solvation molecules, which can be seen from the Na–O radial distribution functions (g_{Na-O}) shown in Supplementary Fig. 5. In addition, one hardly sees water molecules within the alkaline CIP. At the acid interface, by contrast, the protons are well solvated and the CIP is separated from the electrode surface by water molecules. The different cation and water distributions in the acid and alkaline EDLs imply that the CIP corresponds to the inner Helmholtz plane at the alkaline interface but the outer Helmholtz plane at the acid interface, which agrees with previous studies[39–42]. This difference should be associated with the partial loss of the solvation shell of Na^+ cations and the asymmetric H-bonding nature of H_3O^+. At the alkaline interface, a relatively large number of Na^+ cations are brought to the EDL to counterbalance the high density of negative charges at the electrode surface, which makes them partially desolvated. These cations prefer the inner Helmholtz plane location so that the interaction between the alkaline cations and electrode surface can make up for the loss of solvation interaction[39,40]. As for the H_3O^+ cations at the acid interface, they prefer the outer Helmholtz plane location because the water molecules in the layer immediately adjacent to the electrode surface (the inner Helmholtz plane) are all in H-down configurations and thereby serve as the H-bond acceptor sites, which can offer an asymmetric solvation environment that matches well with the asymmetric H-bonding properties of H_3O^+ cations at the outer Helmholtz plane[42]. In addition, the position of the CIP in alkaline media agrees well with that measured through surface X-ray scattering technology[43,44], which rationalizes our simulated EDL structures.

The interfacial distributions of water molecules, represented by the oxygen concentration profiles along the surface normal direction, are further illustrated (Fig. 1c). It is apparent that at the distance of ~3.30 Å away from the Pt surface, both acid and alkaline interfaces exhibit a sharp peak of water concentration, which is within the acid CIP while out of the alkaline CIP, again suggesting that no water molecules are present between the cations and electrode surface at the alkaline interface. As marked by the shaded areas in the figure, both the acid and alkaline interfaces possess a gap zone above the CIP in which the water concentration is fairly low and beyond which the water concentration fluctuates around the bulk value (0.056 mol cm⁻³). The gap zone at the alkaline interface is apparently larger in width and more depleted in water concentration than that at the acid interface. One can imagine
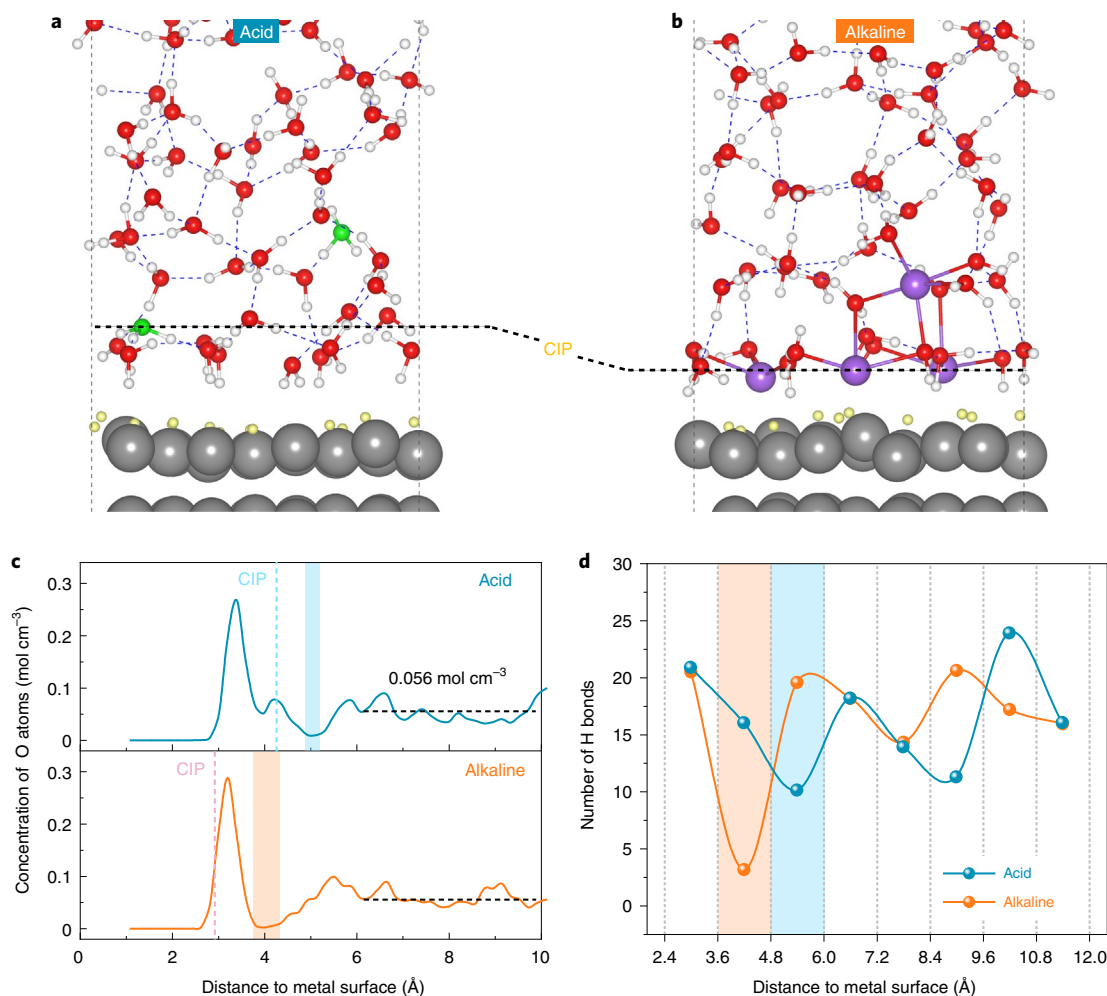
Fig. 1 | EDL structures at acid and alkaline interfaces. a,b, Representative snapshots of the EDL structures at hydrogen evolution potentials on the Pt(111) electrode surface for an acid system (**a**) and alkaline system (**b**). The Pt, O, H, H_3O^+, Na^+ and H_{ad} are coloured in grey, red, white, green, purple and yellow, respectively. The blue dashed lines represent the H bonds. **c**, Concentration distribution profiles of O atoms in water along the surface normal direction. The vertical dashed lines represent the CIPs. The horizontal black dashed lines represent the bulk water concentration (0.056 mol cm^{-3}). **d**, Statistical distribution of the number of H bonds along the surface normal direction. The shaded areas represent the gap zones of interfacial water and H-bond networks.

that the severe depletion of water molecules would reduce the connectivity of the H-bond networks at the alkaline interface, which is verified by the statistical distribution of H bonds along the surface normal direction (Fig. 1d). A region is seen to exist ~4.2 Å away from the Pt(111) surface (orange shading) at the alkaline interface, in which the number of H bonds is significantly diminished as compared with the neighbouring regions. On the contrary, the number of H bonds at the acid interface is similar to that in the bulk region. Such EDL features at the alkaline interface are proved to be independent of surface size (Supplementary Fig. 6). In addition, considering that realistic electrode surfaces under electrochemical conditions often contain plentiful defect and step sites, the alkaline interfaces on the Pt(100) and Pt(553) surfaces at HER potentials have also been simulated to further confirm the scarcity of H-bond networks in the alkaline EDL. As shown in Supplementary Fig. 7, the gap zones of interfacial water are obviously seen for both Pt(100) and Pt(553) surfaces, in which the number of H bonds is also greatly diminished. Such a diminishment in H bonds should be due to the large decrease in the number of solvated water molecules of the crowded CIP cations and the strong interaction between the CIP cations and their solvated water molecules, which significantly reduce the ability of these water molecules to form H bonds with others.

To verify the universality of the discontinuity of H-bond networks in an alkaline EDL in hydrogen electrocatalytic systems including HER and HOR, the alkaline interface on a Pt(111) electrode is further simulated under HOR conditions (Supplementary Fig. 8a). It is apparent that the features of the alkaline interface in the HOR regime agree well with that in the HER regime; namely, the gap zone of interfacial water and the discontinuity of H-bond networks in the EDL are distinctly present (Supplementary Fig. 8b,c). This unequivocally indicates that the discontinuity of H-bond networks in the EDL is a general feature at alkaline interfaces of hydrogen electrocatalytic systems. Although the surface charge densities and electrode potentials between the HER and HOR systems are markedly different, the alkaline EDLs possess fairly similar features (Fig. 1 and Supplementary Fig. 8), implying that the discontinuity of H-bond networks should be mainly attributed to the presence of crowded alkali metal cations, rather than the surface charge densities related to the electrode potentials. It is conceivable that the greatly reduced connectivity of H-bond networks near the electrode surface would severely inhibit the hydrogen electrocatalytic reactions, since the H-bond networks constitute highways for delivering protons to the surface, which, as will be shown in the following, is vital in hydrogen electrocatalysis.
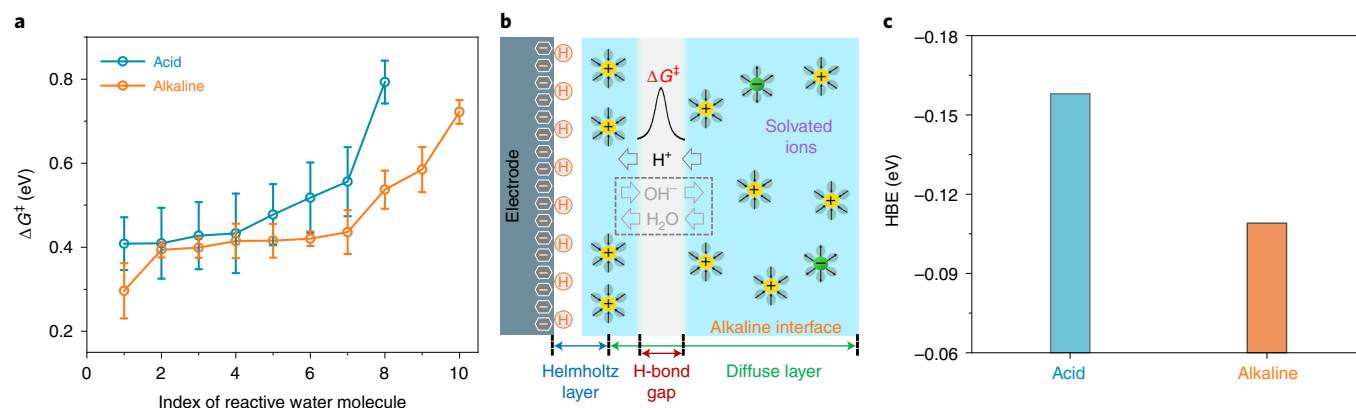
Fig. 2 | Comparison of Volmer barriers and HBEs at acid and alkaline interfaces. a, The calculated free energy barrier $\Delta G^{\ddagger}$ of the individual Volmer reaction for the closest water molecules at the acid and alkaline interfaces. Error bars (s.d.) are calculated based on three individual slow-growth simulations.

b, Schematic diagram of the alkaline EDL structure and the proton transfer from bulk to interface across the H-bond gap. **c**, The calculated HBE values at the acid and alkaline interfaces.

Origin of the great kinetic pH effect in HER/HOR

The HER/HOR essentially involves a hydrogen transfer (HT) process, via the Volmer and/or Heyrovsky reaction, which consists of roughly two HT steps in series: the HT between the electrode surface and the interfacial species closest to it (HT-1), and the HT between the bulk and the closest interfacial species through the H-bond networks in the EDL (HT-2). Taking HER as the example, it has been argued that the great difference between the HER kinetics at acid and alkaline interfaces is due to the different hydrogen sources, namely, hydronium cations (H_3O^+) at the acid interface and water molecules at the alkaline interface. HT through water dissociation is traditionally believed to have a higher energy barrier than that through H_3O^+. As implied in the simulated EDL structures (Fig. 1a,b), the closest hydronium cations (H_3O^+) at the acid interface are separated from the electrode surface by interfacial water molecules. Therefore, it should be the water molecules closest to the electrode surface rather than the H_3O^+ that directly participate in the HT-1 step in acidic HER. Thus, the HER kinetics at the acid and alkaline interfaces may be compared by investigating the HT processes of the water molecules closest to the electrode surface. We consider the Volmer reaction for simplicity. The slow-growth method is used to evaluate the free energy barriers ($\Delta G^{\ddagger}$) of the individual Volmer reaction, with each closest water molecule serving as the direct dissociative reactant to form H_{ad} (Supplementary Fig. 9). At the acid interface, the collective variable (CV) is defined as the combination of several O–H distances connecting the H-bond networks from H_3O^+ to the closest water molecule, while the O–H bond length of the interface water molecule is directly used as the CV in alkaline media (Supplementary Fig. 10). The lateral proton transfer parallel to the surface is also included in the definition of CV at the acid interface (Supplementary Fig. 11), which has been reported to be important for the evaluation of reaction energetics[45]. To ensure the accuracy and reliability of the free energy barrier comparison, the slow-growth simulation for each water molecule has been performed three times independently to obtain the error analysis. In acidic Volmer reactions, the hydronium at CIP transfers H to the dissociated water molecules closest to the electrode surface through the H-bond networks in the EDL (Supplementary Fig. 12); in alkaline reactions, the dissociated water molecules closest to the surface gain H through the H-bond networks in the EDL, and meanwhile a hydroxyl anion (OH^-) is produced in the region out of the CIP (Supplementary Fig. 13). As illustrated in Fig. 2a, surprisingly, the Volmer reactions of various water molecules at the acid interface have higher free energy barriers than those at the alkaline interface. We have also conducted slow-growth simulations for the Volmer reaction at the acid interface by using the O–H bond length of the interface water molecules closest

to the electrode surface as the CV (Supplementary Fig. 14), as we did at the alkaline interface. The results continue to suggest higher free energy barriers at the acid interface than at the alkaline interface. In addition, the alkaline interface with an additional NaOH being inserted into the electrolyte is also simulated (Supplementary Fig. 15), and the results show that the presence of explicit OH^- anions doesn't affect the simulation results or the conclusions drawn from them (Supplementary Fig. 16), which contradicts the long-established belief that the alkaline HT processes should be more energy demanding than the acidic ones through the dissociation of interfacial hydronium[21]. When considering the EDL structures, however, the lower free energy barrier of the individual HT-1 step in alkaline conditions becomes reasonable.

As mentioned above, it is the water molecules closely neighbouring the electrode surface rather than the H_3O^+ cations that directly act as the HT sources to form H_{ad} at the acid interface. That is, the HT-1 steps at both the acid and alkaline interfaces should be the dissociation of the closest water molecules. At the alkaline interface, these water molecules are strongly polarized by cations, which will significantly weaken the O–H bond strength and thereby lower the dissociation barrier. The facilitated reactivity by the interacting metal cations has been corroborated experimentally[46]. In addition, the electrode surface with a much higher negative charge density should strongly attract the hydrogen atoms in water, which further facilitates the breakage of the O–H bond of the nearby water molecules. Consequently, the approximately two orders of magnitude lowering in the alkaline HER activity cannot be simply attributed to the change of H source from hydronium ions to water molecules.

Besides the HT from the closest interfacial water molecules to the electrode surface (HT-1), the HT from the bulk region to interfacial water molecules through the H-bond networks in the EDL (HT-2) is also essential to the whole HER process. As revealed in the simulated EDL structures (Fig. 1d) and the corresponding schematic diagram (Fig. 2b), the number of H bonds is significantly diminished in the region near the alkaline Helmholtz plane. The scarcity of H bonds drastically reduces the HT channels, thereby leading to significant HT congestion around the Helmholtz plane. On the other hand, the insufficient supply of protons to the inner interface may result in the accumulation of OH^- ions, which can further increase the free energy barrier of the water dissociation. The present finding highlights immense opportunities to regulate the electrochemical reaction kinetics in an alkaline environment by optimizing the interfacial water distribution and the connectivity of H-bond networks. It can explain well why bringing down the electrode PZC[4,17] and/or adding protic ionic liquids (or organic molecules)[36,38] as the electrolyte components can be effective strategies to improve the
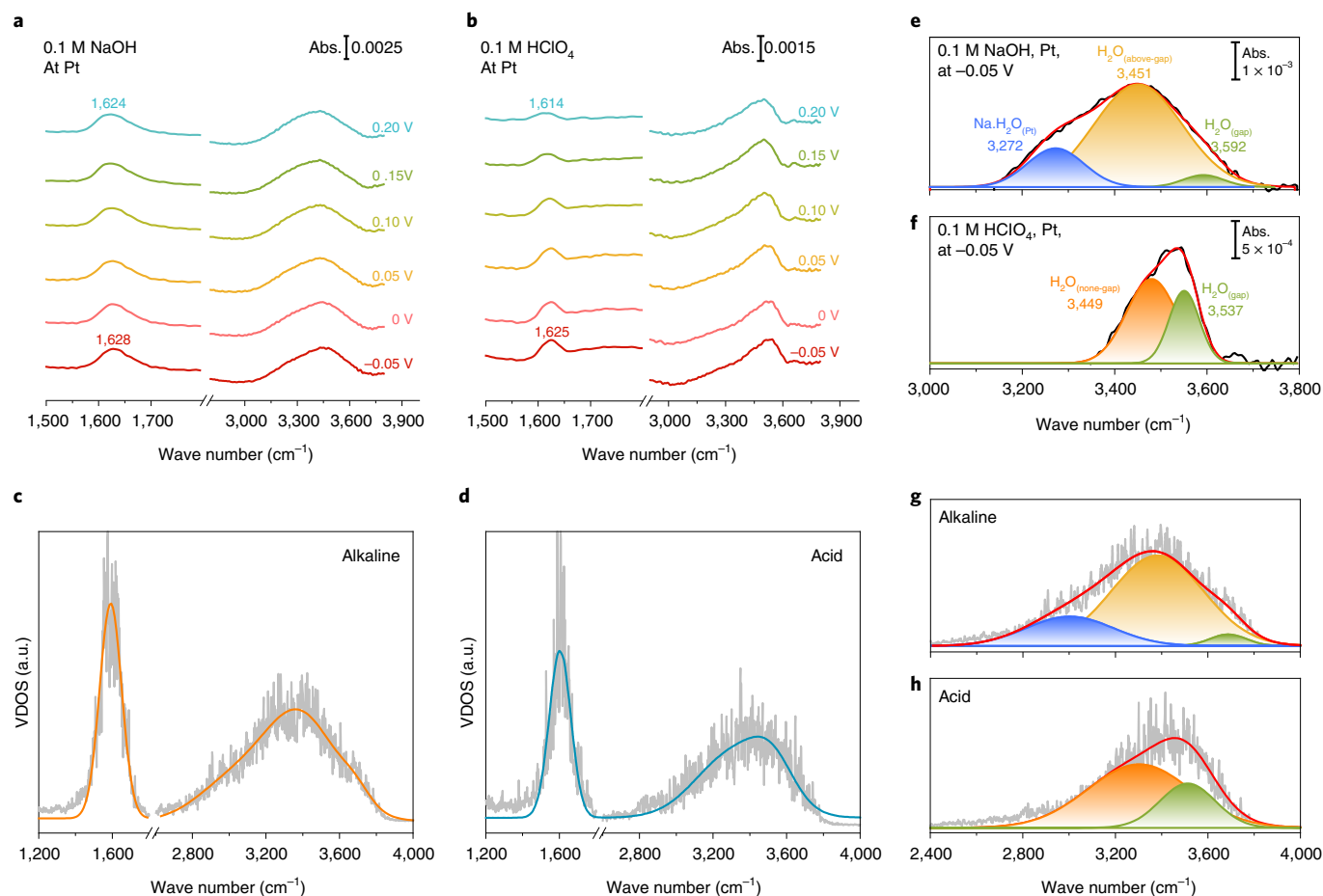
Fig. 3 | Infrared spectra. a,b, In situ SEIRAS spectra recorded at potentials from 0.20 V to −0.05 V for a Pt electrode in Ar-saturated solutions of 0.1 M NaOH (**a**) and 0.1 M HClO₄ (**b**). Spectra subtracted by the reference spectrum taken at 0.90 V and 0.50 V for alkaline and acid systems, respectively. The spectra recorded at potentials from 1.10 V to −0.05 V are available in Supplementary Fig. 21. **c,d,** The computational VDOS (grey jagged lines) of interfacial water molecules within ~6.6 Å from the electrode surface at alkaline (**c**) and acid (**d**) interfaces. The orange and blue lines are the Gaussian fittings of computational VDOS. **e,f,** Deconvolution of the experimental O–H stretching vibration peak at −0.05 V (versus RHE) in NaOH (**e**) and HClO₄ (**f**) solutions. **g,h,** Deconvolution of the computational O–H stretching vibration peak at alkaline (**g**) and acid (**h**) interfaces.

hydrogen electrocatalytic kinetics. The former can reduce the negative charge density on the electrode surface, thereby decreasing the cation concentration required to establish the EDL and eventually improving the interfacial water distribution and H-bond networks. The latter can construct and strengthen the interfacial H-bond networks and serve as the role of proton pump to efficiently transfer the protons in the EDL.

We also evaluated the HBEs at acid and alkaline interfaces, through the calculation method introduced in Supplementary Note 1 and Supplementary Fig. 17. Figure 2c shows that the hydrogen binding strength at the acid interface is stronger than that in an alkaline environment, agreeing well with the recent voltammetric and spectroscopic experiments[17–19]. This demonstrates that the pH-dependent HER kinetics cannot be described aptly by the difference in hydrogen binding strength.

Rationalization of the H-bond network gap using in situ SEIRAS

To corroborate the H-bond network gap in the alkaline EDL, we conducted in situ SEIRAS measurements in ATR mode and compared the experimental vibration responses with the computational VDOS of interfacial water molecules in the simulated EDLs. The ATR-SEIRAS results, given in the form of difference spectra, usually show an excellent surface enhancement effect and sensitivity within ~5–10 nm from

the electrode surface[47], thus enabling the accurate detection of the EDL structures at electrochemical interfaces.

A chemically deposited Pt thin film electrode is used as the working electrode in SEIRAS. The typical cyclic voltammograms of the Pt thin film electrode in 0.1 M HClO₄ and NaOH solutions are shown in Supplementary Fig. 18, and both are identical to those of polycrystalline Pt in the corresponding environments[18]. Atomic force microscopy images show that the Pt thin film electrode possesses a rough surface with islands composed of Pt nanoparticles (Supplementary Fig. 19). In addition, the spectrum measured in CO-saturated 0.1 M HClO₄ solution exhibits only two peaks centred at 2,073 cm⁻¹ and 1,871 cm⁻¹ (Supplementary Fig. 20), which are assigned to the C–O stretching modes of CO adsorbed on the top and bridge sites of Pt surface, respectively[48,49]. This indicates that the Au substrate is completely covered by the deposited Pt film and thus creates negligible interference in the infrared spectra measurement.

Figure 3a,b show the in situ SEIRAS spectra of interfacial water molecules on Pt at various potentials in Ar-saturated 0.1 M NaOH and HClO₄ solutions, respectively. The spectra are given in the form of difference spectra, with that collected at potentials of 0.9 V in alkaline and 0.5 V in acid as the references, due to such potentials having been widely used in previous reports[18,50,51]. Moreover, we find that the spectra recorded in a wide potential range (from 1.10 V to −0.05 V) exhibit approximately a
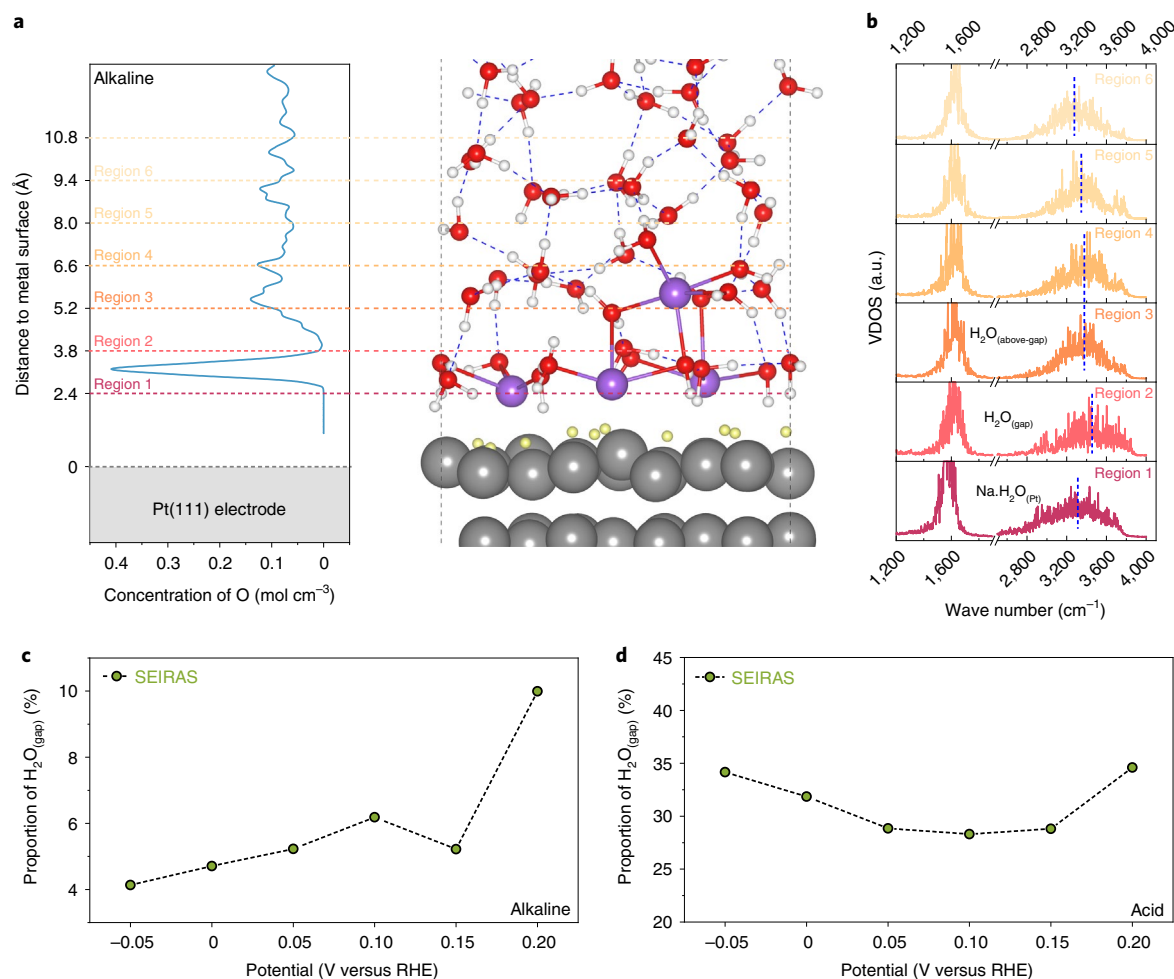
Fig. 4 | Spectroscopic analysis of different interfacial water molecules. a, Schematic diagram of region division for the alkaline system. Region 2 represents the gap of H-bond networks. **b**, The computational VDOS of the water molecules at various distances from the electrode surface under alkaline conditions.

The blue dashed lines represent the peak positions. **c**,**d**, Potential-dependent proportion of $H_2O_{(gap)}$ from in situ SEIRAS spectra at alkaline (**c**) and acid (**d**) interfaces.

watershed at 0.9 V in alkaline and 0.5 V in acid (Supplementary Fig. 21), which implies that the water molecules in EDLs undergo a substantial change in adsorption configurations[49]. Thus, taking 0.9 V in alkaline and 0.5 V in acid as the reference potentials can avoid the interference of a configuration change on the difference spectra of interfacial water molecules. Although taking the spectra at any potentials below 0.9 V as the reference in alkaline may not involve the interference of the water configuration change, significant accumulation of cations at the inner Helmholtz plane already occurs if the potential deviates too much from the PZC, for example, 0.5 V versus RHE (the PZC is around 1.0 V versus RHE in alkaline)[29]. This will result in the partial loss of spectral information of interfacial water associated with the cation crowding effect in an alkaline system.

In addition, we have calculated the VDOS values for the interfacial water molecules within ~6.6 Å from the Pt surface in the AIMD-simulated EDLs at alkaline and acid interfaces. As shown in Fig. 3c,d, the computational spectra possess very similar shapes to that of the experimental SEIRAS spectra. Specifically, the O–H stretching peak of interfacial water displays a broader and symmetric shape in an alkaline system but a more asymmetric shape extending towards the lower frequency region in an acidic system. In addition, the experimental O–H stretching peak in NaOH solution can be deconvoluted into three distinct components through Gaussian fitting (Fig. 3e and Supplementary Fig. 22a); in HClO$_4$ solution, the O–H stretching band can only be resolved into two

components (Fig. 3f and Supplementary Fig. 22b). The deconvolution of the computational VDOS of the O–H stretching mode exhibits nearly identical features (Fig. 3g,h). These consistencies not only indicate that the ATR-SEIRAS signals were mainly derived from the first few layers of water molecules close to the electrode surface, but also confirm that the AIMD-simulated EDL structures reasonably represent structures at the real electrochemical interfaces. Therefore, the existence of a H-bond network gap at the alkaline interfaces can be proven.

To further understand the experimental and computed vibrational spectra, the VDOS of interfacial water molecules at different distances from the electrode surface have been calculated. Figure 4a shows the schematic diagram of the division into regions, in which region 2 is the gap region of H-bond networks. As shown in Fig. 4b, the O–H stretching vibration peak of water molecules at the alkaline interface exhibits first a blueshift and then a redshift with the location moving away from the electrode surface. The water molecules located in the gap region (denoted $H_2O_{(gap)}$) have the highest O–H stretching vibration frequency, while those above the gap region (denoted $H_2O_{(above-gap)}$) and those nearest to the electrode surface (denoted $Na.H_2O_{(Pt)}$) have the second and lowest O–H stretching vibration frequencies, respectively. The blueshift of the O–H stretching mode of water within the gap region can be explained with the presence of a quasi-dangling OH group, as suggested by the sum frequency generation spectra[52]. In addition, these features of theoretical spectra seem to agree well with
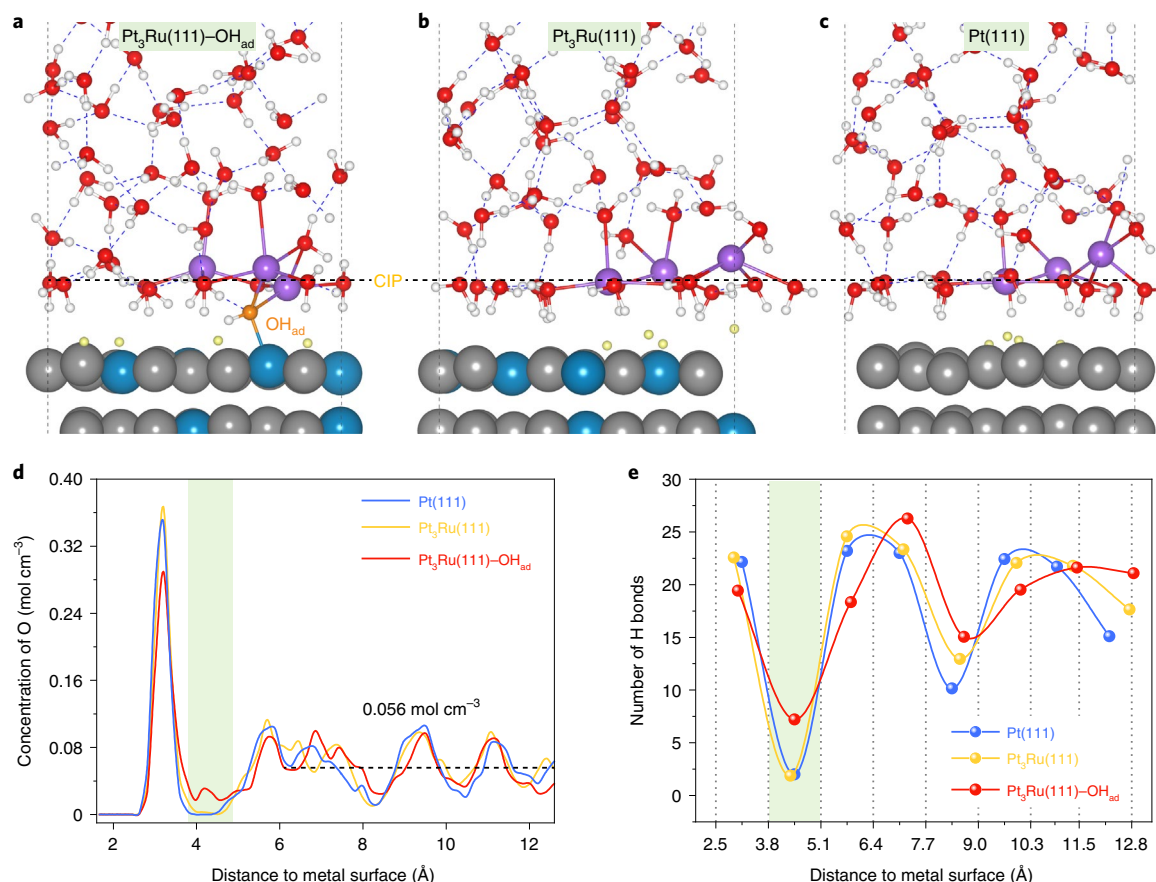
Fig. 5 | Improvement of the connectivity of interfacial H-bond networks by OH$_{ad}$. a–c, Representative snapshots of the AIMD-simulated interface structures on a Pt$_3$Ru(111) electrode with (**a**) and without (**b**) OH adsorption, and that on a Pt(111) electrode (**c**) at hydrogen oxidation potentials. The coverage of H$_{ad}$ is set at 0.25 ML (defined per surface Pt atom). The Pt, Ru, H, Na$^+$, O of water, O of OH$_{ad}$ and H$_{ad}$ are coloured in grey, blue, white, purple, red, orange and yellow, respectively. **d**, The concentration distribution profiles of O atoms of water along the surface normal direction. **e**, Statistical distribution of the number of H bonds along the surface normal direction. The green shadings represent the gap regions of interfacial water and H-bond networks.

the above experimental observation that the O–H stretching spectra for water molecules at the alkaline interface can be deconvoluted into three distinct components. Consequently, the high wave-number component (green shading), main component (yellow shading) and low wave-number component (blue shading) in Fig. 3e,g are associated with H$_2$O$_{(gap)}$, H$_2$O$_{(above-gap)}$ and Na.H$_2$O$_{(Pt)}$, respectively. In an acidic system, the H$_2$O$_{(gap)}$ gives a slightly higher theoretical O–H stretching wave number, while the other interfacial water molecules (denoted as H$_2$O$_{(none-gap)}$) exhibit nearly the same O–H stretching vibration frequency (Supplementary Fig. 23), which seems to explain well why the experimental spectra for the acidic system can only be deconvoluted into two distinct components (Fig. 3f,h). These results reveal that the H$_2$O$_{(gap)}$ usually has a stronger O–H stretching vibration when comparing to the adjacent water molecules, which should further suggest the relative scarcity of H-bond networks in the gap region. In addition, the partial VDOS of interfacial water molecules at various distances from the electrode are analysed, to verify the accuracy and reliability of the above deconvolutions and peak assignments of the experimental SEIRAS and theoretical VDOS. As shown in Supplementary Figs. 24 and 25, it is apparent that either at the alkaline interface or the acidic interface, the variation trends of the O–H stretching vibration frequencies obtained from the partial VDOS of O atoms at different distances from the electrode surface are fully in line with those obtained from the partial VDOS of H atoms and the total VDOS (Fig. 4b and Supplementary Fig. 23b), which further rationalizes the deconvolutions of the experimental SEIRAS and theoretical VDOS and their peak assignments.

To further compare the degrees of the H-bond network gap at alkaline and acidic interfaces, the potential dependences of O–H stretching vibration frequencies of each type of interfacial water molecules at alkaline and acidic interfaces are compared (Supplementary Fig. 26). In addition to the frequency shift due to the vibrational Stark effect[53], the difference in the O–H stretching wave numbers between H$_2$O$_{(gap)}$ and H$_2$O$_{(above-gap)}$ in an alkaline system (~150 cm^{-1}) is much higher than that between H$_2$O$_{(gap)}$ and H$_2$O$_{(none-gap)}$ in an acidic system (~72 cm^{-1}), demonstrating the much more severe scarcity of H-bond networks in an alkaline EDL. On the other hand, the potential-dependent proportions of the deconvoluted peak for H$_2$O$_{(gap)}$ in alkaline and acidic environments have been analysed. The proportion of H$_2$O$_{(gap)}$ molecules at the alkaline interface gradually decreases with decreasing potential (Fig. 4c), which should be due to the more serious depletion of water molecules and H-bond networks caused by the increased Na$^+$ concentration in the EDL. By contrast, the proportion of H$_2$O$_{(gap)}$ molecules at the acidic interface not only is much higher than that at the alkaline interface, but also shows negligible change with potential (Fig. 4d), which suggests that the discontinuity of H-bond networks is almost negligible in the acidic system. To check whether the choice of reference spectra affects the above discussions and conclusions, the spectra recorded at 0.90 V was used as the reference in acid. The difference spectra obtained have similar shapes but a larger line-width (Supplementary Fig. 27a) as compared to that shown in Fig. 3b. However, as shown in Supplementary Fig. 27b–d, the O–H stretching bands can only be resolved into two components and exhibit the same

features as that shown in Fig. 4d and Supplementary Fig. 26, which confirms that the discontinuity of H-bond networks in the EDL is evident in alkaline, while being almost negligible in acid. Finally, the analysis of the experimental spectra and its correlations with the EDL structures are not unassailable, and we should be fairly cautious, because there still exist great challenges and limitations in high-quality acquisition of interface spectroscopy signals, spectral peak deconvolutions and assignments, and so on. However, the combination of experimental and computational spectra can provide an avenue for exploring electrochemical interface structures more accurately.

Improving the H-bond network connectivity by OH adsorption

Numerous recent studies have revealed that alloying Pt with Ru can significantly enhance the HOR/HER kinetics in alkaline electrolyte, which has been ascribed to the facilitated water formation/dissociation due to the increased OH/H_2O adsorption on the more oxophilic Ru atoms[20,27]. As shown in the previous section, the water dissociation may not be the major cause of the decreased activity of Pt in the hydrogen electrocatalytic reaction in alkaline electrolyte, while the connectivity of H-bond networks near CIP may be a dominant factor of the kinetic pH effect. Therefore, we investigate the effect of OH adsorption on the connectivity of interfacial H-bond networks, using $Pt_3Ru(111)$ as a model surface. First, the alkaline interfaces on the $Pt_3Ru(111)$ electrodes with and without OH adsorption in the HOR scenario are simulated (Fig. 5a,b), and the electrode potentials at pH = 14 are calculated as -0.40 V and -0.14 V, respectively. Meanwhile, the interface on the Pt(111) electrode under alkaline HOR conditions is also shown for comparison (Fig. 5c and Supplementary Fig. 8). As shown in Fig. 5d,e, the distributions of water concentration and number of H bonds at the interface on the $Pt_3Ru(111)$ electrode without OH adsorption are very similar to those on the Pt(111) electrode, both exhibiting fairly low water concentrations and scarce H bonds within the green shaded region (namely, the gap zone above the CIP). By contrast, at the interface on the $Pt_3Ru(111)$ electrode with OH adsorbed on Ru sites, the water concentration within the green shaded region is apparently higher, which therefore leads to the remarkable increase in the number of H-bonds. This suggests that the OH adsorption can significantly increase the water connectivity and improve the H-bond networks in the EDL. Then, to further verify this role of OH adsorption, the alkaline interfaces on $Pt_3Ru(111)$ and stepped Ru–Pt(553) electrodes in the HER scenario are also simulated. The results indicate that the interfacial water concentration and number of H bonds in the gap zone increase significantly on the electrodes with OH_{ad} (Supplementary Figs. 28 and 29). In addition, in situ SEIRAS measurements are also performed for the Pt–Ru electrode in alkaline media (Supplementary Fig. 30). The spectral results show that, compared to that on the Pt electrode, the proportion of $H_2O_{(gap)}$ molecules at the alkaline interface on the Pt–Ru electrode becomes distinctly higher and the O–H stretching band of $H_2O_{(gap)}$ is redshifted by -15 cm^{-1} (Supplementary Fig. 31), which suggests that the water concentration in the gap zone is increased and the H-bond networks in the EDL are enhanced accordingly. The combination of in situ SEIRAS experiments and AIMD simulations thus provides a solid support for the role of OH adsorption in improving the connectivity of interfacial water distribution and H-bond networks in an alkaline EDL on Pt–Ru. Furthermore, all the above results imply that the proposed connectivity of H-bond networks in the EDL could serve as the universal descriptor for the kinetic pH effect in both the HER and HOR.

To understand this phenomenon, the EDL structures of the interfaces on $Pt_3Ru(111)$ electrodes with and without OH adsorption are carefully compared. First, on the $Pt_3Ru(111)$ electrode with OH adsorption, the Na^+ ions mainly gather around the adsorbed OH species due to the coordination interaction, rather than being more spread over the electrode surface as on bare $Pt_3Ru(111)$, as shown in Fig. 5a,b and Supplementary Fig. 32. The aggregation of cations around OH would increase the space for water molecules in the CIP region. On the other hand, the coordination between Na^+ ions and adsorbed OH leaves more free water

molecules (Supplementary Fig. 32), which possess a stronger ability to form an H bond with others. Several recent studies have reported that adding more cations into alkaline solution can improve the HER activity of PtNi, Pt(111)/Ni(OH)$_2$ and other electrodes, and different models, for example, 2B theory and bi-functional theory[6,54,55], have been proposed to explain these experimental observations. These results, at first sight, seemingly contradict the current viewpoint that the crowded cations inhibit the HER/HOR by causing the interfacial H-bond gap. However, these observations are mainly obtained on electrodes that have considerable surface affinity for OH species[54–56]. As shown here, the presence of OH_{ad} can significantly offset the depletion effect of crowded cations on the H-bond networks. With the significant improvement of H-bond networks, the other effects of cations on the electrocatalytic kinetics may become important, for example, through the recently proposed 2B and bi-functional mechanisms. Thus, the observed increase in the activity of the OH-adsorbing electrodes with increasing cation concentrations somewhat supports our proposition that OH adsorption enhances the alkaline HER/HOR activity of Pt-based alloys through offsetting the depletion effect of cations on the H-bond networks in EDLs. In addition, the cation concentrations may also impact the HER kinetics by changing the compactness of the EDLs. The cations may have multiple and complicated roles in the kinetics of electrocatalytic reactions, which deserve further detailed studies.

In addition, Synder et al. have shown recently that the adsorption of caffeine on the Pt(111) electrode could significantly enhance the HER/HOR kinetics in alkaline[57], but the mechanism is still unclear. In this regard, the alkaline interface on the Pt(111) electrode with an adsorbed caffeine molecule is investigated. As illustrated in Supplementary Fig. 33, the adsorbed caffeine molecule can coordinate with the Na^+ cations and therefore lead to the formation of a water domain with rich H-bond networks at the interface, thereby facilitating the alkaline HER/HOR. This explanation should also be supported by the experimental observation that caffeine adsorption enhances only the alkaline HER/HOR while inhibiting the acidic HER/HOR. Specifically, due to the good connectivity of H-bond networks in an acidic EDL, the introduction of caffeine would decrease the kinetics mainly by blocking the active sites. The mechanism with which the caffeine improves the hydrogen electrocatalytic kinetics is similar to that of OH_{ad}, which further suggests the dominating role of the connectivity of H-bond networks in the kinetic pH effect of hydrogen electrocatalysis.

Conclusions

The roles of the EDL structure in the kinetic pH effect of hydrogen electrocatalysis on Pt-based electrodes have been elucidated by combining AIMD simulations and in situ SEIRAS measurements. The results suggest that neither the hydrogen adsorption strength nor the water dissociation/formation barrier is responsible for the greatly reduced kinetics of hydrogen electrocatalysis in alkaline solution; rather, the water distribution and the connectivity of H-bond networks in the EDL play a dominant role. We also revealed an unanticipated role of the adsorbed OH in impacting the electrocatalytic activity, namely, by modulating the water connectivity and improving the H-bond networks in the EDL, rather than by merely affecting the energetics of surface reaction steps (such as water dissociation/formation). Our findings highlight the significance of EDL microstructures in the electrocatalytic reaction kinetics and could provide innovative guidance for designing pH-oriented electrocatalysts. This study may also offer a research model for reference in the future exploration of atomic structures of electrochemical interfaces by combining experimental and computational spectroscopies.

Methods
Computations and models
All AIMD simulations are performed using the Vienna Ab initio Simulation Package, a plane-wave pseudopotential code[58,59].

The Perdew–Burke–Ernzerhof functional within the generalized gradient approximation is applied to evaluate the exchange and correlation energies[60]. The wavefunctions are expanded up to a cut-off energy of 400 eV, and the first-order Methfessel–Paxton scheme with a smearing width of 0.2 eV is employed. The van der Waals interaction is considered through the semi-empirical D3 dispersion correction scheme of Grimme[61]. Non-spin polarization is included in all simulations, because it has almost no effect on the overall energies. The time step is set as 1.0 fs, and only the gamma point of the Brillouin zone with no consideration of symmetry is used. A Nose–Hoover thermostat is applied to keep the temperature of the canonical ensemble at 298 K.

The Pt(111)/water interface is modelled by adding 60 water molecules above a four-layer 4 × 4 orthogonal Pt(111) slab with a surface area of 1.10 nm^2. The thickness of the water film and vacuum layer are ~1.6 nm and ~2.4 nm, respectively, and the size of the whole simulation box is ~4.9 nm along the z axis. To fully equilibrate the H-bond networks of the water layer and reduce the AIMD simulation time, we first perform a 250 ps classical molecular dynamics simulation with a reactive force field at 298 K by using the Large-scale Atomic/Molecular Massively Parallel Simulator with user package Reax/C (refs. [62,63]). The Pt–O–H reactive force field developed by Shin et al. is applied to describe the interaction between the water and metal surface[64]. The pre-equilibrated Pt(111)/water interface given by the classical molecular dynamics simulations is used as the initial configuration to perform the AIMD simulations. All AIMD trajectories are sampled for runtimes of up to 15–25 ps to ensure that the interface systems are well equilibrated, and the snapshots in the last 10 ps are implied for statistical analyses. For other flattened and stepped Pt surfaces and Pt–Ru systems, the interface models are similar. The atomic coordinates of the initial and final configurations of the trajectories in the AIMD simulations for the systems shown in Fig. 1 and Fig. 5 are provided as Supplementary Data. The work functions (∅) of various metal/electrolyte interfaces are calculated with a standard approach, that is, according to the energy difference between the vacuum level (E_{vac}) and Fermi level (E_F). The energy value of E_{vac} is extracted from the planar-averaged electrostatic potential profile, with 10^{-5} e$^-$ Å^{-3} being chosen as the cut-off value of electron density. This cut-off method is similar to that in the implicit solvation/electrolyte models, in which a cut-off charge density is set to determine the boundary of the dielectric cavity[65]. Then, according to $U_{SHE} = ∅ - ∅_{SHE}$, where $∅_{SHE}$ is the work function of the standard hydrogen electrode (SHE; 4.44 V)[66], the PZC of the Pt(111)/water interface is calculated as ~0.21 V, a value well in line with the experimental measurements and other molecular dynamics simulations[67–69]. The VDOS values of interfacial water molecules (within ~6.6 Å away from the Pt surface) were calculated by the Fourier transformation of the velocity auto-correlation functions in the AIMD trajectories.

To simulate the acidic and alkaline environments, we explicitly insert hydronium ion (H$_3$O$^+$) and Na ion (Na$^+$), respectively, into a water film. These ions are initially positioned ~3–4 Å away from the Pt(111) surface to model the compact Helmholtz layer. The Gouy–Chapman diffusion layer is omitted when considering the relatively high ion concentration of electrolytes in experiments. The co-ions are also neglected because the electrode surfaces should be highly charged at HER potentials and the co-ions should be repelled away from the Helmholtz plane. Meanwhile, since the whole system is kept charge neutral, the same number of electrons as that of inserted ions will be introduced into the metal surface to tune the Fermi level. Thus, we can vary the number of inserted ions to control the surface charge density and then the electrode potential to reach the potential range of hydrogen evolution. The electrode potentials with respect to that of the RHE are estimated according to $U_{RHE} = \frac{∅ - ∅_{SHE}}{e} + 0.059 \times pH$, where e is the electron charge.

In addition, the hydrogen adsorption intermediate (H$_{ad}$) is taken into account to describe the surface state of the Pt(111) electrode under the hydrogen evolution potential as truthfully as possible, and the coverages are set as 0.88 monolayer (ML, defined per surface Pt atom) and 0.63 ML for acidic and alkaline systems, respectively, according to previous experimental results[70]. The peculiar advantage of our theoretical model lies in that the electrode potential, the properties and ion concentrations of acidic/alkaline EDLs and the species adsorbed on the electrode surface are approximately self-consistent, which will provide a reasonable description of the pH-dependent reaction kinetics.

The slow-growth approach[71], within the constrained molecular dynamics framework, is utilized to calculate the free energy profile of the H$_{ad}$ formation process (Volmer step), namely the H$_3$O$^+$ dissociation (H$_3$O$^+$ + e$^-$ ↔ *H + H$_2$O) in acidic solution and H$_2$O dissociation (H$_2$O + e$^-$ ↔ *H + OH$^-$) in alkaline solution. The increment of 0.0008 Å fs^{-1} for CV is set to drive the chemical reactions. Three independent simulations are performed for each reaction to ensure the accuracy and reliability of the free energy barrier results. In addition, all constrained molecular dynamics simulations are carried out under constant charge conditions, meaning that the work functions will change along the reaction pathway. To gain the constant potential results and compare with experiments, the correction procedure proposed by Chan and Nørskov is employed to remove any artefacts due to work function changes during the simulation[72,73]. The detailed principles of the slow-growth approach and constant potential correction can be found in Supplementary Notes 2 and 3.

Preparation of Pt and Pt–Ru thin film electrodes

The Pt thin film working electrode was prepared by a typical two-step deposition method[18,74], involving the chemical deposition of a Au thin film on a hemispheric Si prism followed by the galvanostatic electrodeposition of a Pt thin film on the Au substrate. Before the chemical deposition of Au, the Si prism was first polished gradually using 1.0, 0.3 and 0.05 μm Al$_2$O$_3$ powder for about 30 min until the surface became totally hydrophobic, and then sonicated and rinsed several times with acetone/ethanol (Sinopharm Chemical Reagent, analytical reagent grade (AR)) mixed solution (volume ratio, v/v = 1:1) and double deionized–distilled water (ULUPURE, 18.2 MΩ). After that, the hydrophobic and clean Si prism underwent hydroxylation treatment with piranha solution (the volume ratio between concentrated H$_2$SO$_4$ and 30% H$_2$O$_2$ is 1:1) for 20 min and then was sonicated with distilled water several times. The infrared reflection plane of the Si prism was then dried by Ar (ultra-high purity grade) flow and treated by 40% NH$_4$F (Sinopharm Chemical Reagent, AR) for 2 min to make the surface be terminated with hydrogen. The thin Au film was then deposited on the hydrogen-terminated surface by immediately immersing this plane into a mixture of 9.2 ml Au plating solution and 124 μl 50% HF solution (Sinopharm Chemical Reagent, AR) at 55–60 °C for 6 min. A voltmeter was used to measure the conductivity of the Au film, showing an ohmic resistance lower than 10 Ω. The Au-coated prism was mounted into a homemade spectro-electrochemical cell as the working electrode; a calibrated saturated calomel electrode (SCE) was assembled near the working electrode via a Luggin capillary as the reference electrode; and a Pt mesh with a size of 0.8 cm × 1.0 cm was used as the counter electrode. The Au film was electrochemically cleaned with cyclic voltammetry between 0.0 and 1.4 V (versus SCE) with a scan rate of 50 mV s^{-1} in the Ar-saturated 0.1 M HClO$_4$ (KESHI, general reagent grade (GR)) solution until a repeatable cyclic voltammetry curve was obtained. After rinsing with sufficient water, electrodeposition of the Pt thin film was carried out in an Ar-saturated solution of 4 mM H$_2$PtCl$_6$ (Kunming Sino-Platinum, >98%) plus 0.7 M Na$_2$HPO$_4$ (Aladdin Chemicals, GR) at a current density of −0.75 mA cm^{-2} for 900 s followed by −0.4 mA cm^{-2} for 480 s. The prepared Pt thin film was carefully washed with distilled water several times and used immediately. The Ru-modified Pt film electrode was prepared by immersing the preprepared Pt film electrode in a 1 mM RuCl$_3$ (Aladdin; Ru content, 45–55%) plus 50 mM H$_2$SO$_4$ (Sinopharm Chemical Reagent, GR) solution for 2 min, according to previous reports[27,50,54,75].

In situ SEIRAS experiments

To conduct SEIRAS measurements, a Hg/HgO electrode and a home-made RHE were used as the reference electrodes in 0.1 M NaOH (Aladdin Chemicals, 99.9%) and 0.1 M $HClO_4$ solutions, respectively. A Fourier transform infrared spectrometer equipped with a liquid-nitrogen-cooled mercury cadmium telluride detector was used for the SEIRAS measurements and operated at a resolution of 8 cm^{-1}. Unpolarized infrared radiation from an Elema source was focused at the reflection plane with an incident angle of ~60°, and the totally reflected radiation was detected. All spectra in this work were shown as absorbance ($-\log(R/R_0)$), where R and R_0 represents the sample and reference spectra, respectively.

Electrochemical measurements

In all electrochemical and spectroscopic measurements, a PARSTAT electrochemical workstation (VersaSTAT 3F) was used. All electrode potentials have been converted to the RHE scale. Before in situ ATR-SEIRAS measurements, the prepared Pt and Pt–Ru thin film working electrodes were cycled in the corresponding electrolyte (Ar-saturated 0.1 M $HClO_4$ or 0.1 M NaOH) between 0.02 V and 1.2 V at a scanning rate of 100 mV s^{-1} for two cycles to get a clean surface. Then the cyclic voltammetry curves in acidic and alkaline solutions were recorded at 10 mV s^{-1}. To collect the infrared spectra, the Pt and Pt–Ru working electrodes were initially kept at 1.2 V for 10 s, and then the potential was linearly swept from 1.2 V to –0.05 V at a scanning rate of 5 mV s^{-1}, during which the infrared spectra were collected using the rapid-scan mode of OPUS software. Each spectrum was co-added by 44 single spectra with a resolution of 8 cm^{-1} and spanned a potential window of 50 mV.

Data availability

Representative data and extended datasets that support the findings reported in this study are available in the manuscript and the Supplementary Information. The data in the figures shown in the main text and the atomic coordinates of the initial and final configurations of the trajectories in the AIMD simulations are provided as supplementary files. Additional data are available from the corresponding author upon reasonable request.

References

1. Chow, J., Kopp, R. J. & Portney, P. R. Energy resources and global development. *Science* **302**, 1528–1531 (2003).
2. Turner, J. A. Sustainable hydrogen production. *Science* **305**, 972–974 (2014).
3. Inzelt, G. Milestones of the development of kinetics of electrode reactions. *J. Solid State Electrochem.* **15**, 1373–1389 (2011).
4. Huang, J., Li, P. & Chen, S. Quantitative understanding of the sluggish kinetics of hydrogen reactions in alkaline media based on a microscopic Hamiltonian model for the Volmer step. *J. Phys. Chem. C* **123**, 17325–17334 (2019).
5. Sheng, W., Gasteiger, H. A. & Shao-Horn, Y. Hydrogen oxidation and evolution reaction kinetics on platinum: acid vs alkaline electrolytes. *J. Electrochem. Soc.* **157**, B1529–B1536 (2010).
6. Subbaraman, R. et al. Enhancing hydrogen evolution activity in water splitting by tailoring Li^+-Ni(OH)$_2$-Pt interfaces. *Science* **334**, 1256–1260 (2011).
7. Durst, J. et al. New insights into the electrochemical hydrogen oxidation and evolution reaction mechanism. *Energy Environ. Sci.* **7**, 2255–2260 (2014).
8. Zheng, Y., Jiao, Y., Vasileff, A. & Qiao, S. Z. The hydrogen evolution reaction in alkaline solution: from theory, single crystal models, to practical electrocatalysts. *Angew. Chem. Int. Ed.* **57**, 7568–7579 (2018).
9. Strmcnik, D., Lopes, P. P., Genorio, B., Stamenkovic, V. R. & Markovic, N. M. Design principles for hydrogen evolution reaction catalyst materials. *Nano Energy* **29**, 29–36 (2016).
10. Sheng, W. et al. Correlating hydrogen oxidation and evolution activity on platinum at different pH with measured hydrogen binding energy. *Nat. Commun.* **6**, 5848 (2015).
11. Zheng, J., Sheng, W., Zhuang, Z., Xu, B. & Yan, Y. Universal dependence of hydrogen oxidation and evolution reaction activity of platinum-group metals on pH and hydrogen binding energy. *Sci. Adv.* **2**, e1501602 (2016).
12. Giles, S. A. et al. Recent advances in understanding the pH dependence of the hydrogen oxidation and evolution reactions. *J. Catal.* **367**, 328–331 (2018).
13. Zheng, J., Nash, J., Xu, B. & Yan, Y. Perspective—towards establishing apparent hydrogen binding energy as the descriptor for hydrogen oxidation/evolution reactions. *J. Electrochem. Soc.* **165**, H27 (2018).
14. Cheng, T., Wang, L., Merinov, B. V. & Goddard, W. A. III Explanation of dramatic pH-dependence of hydrogen binding on noble metal electrode: greatly weakened water adsorption at high pH. *J. Am. Chem. Soc.* **140**, 7787–7790 (2018).
15. Chen, X., McCrum, I. T., Schwarz, K. A., Janik, M. J. & Koper, M. T. Co-adsorption of cations as the cause of the apparent pH dependence of hydrogen adsorption on a stepped platinum single-crystal electrode. *Angew. Chem. Int. Ed.* **56**, 15025–15029 (2017).
16. Janik, M. J., McCrum, I. T. & Koper, M. T. On the presence of surface bound hydroxyl species on polycrystalline Pt electrodes in the "hydrogen potential region" (0-0.4 V-RHE). *J. Catal.* **367**, 332–337 (2018).
17. Ledezma-Yanez, I. et al. Interfacial water reorganization as a pH-dependent descriptor of the hydrogen evolution rate on platinum electrodes. *Nat. Energy* **2**, 17031 (2017).
18. Zhu, S., Qin, X., Yao, Y. & Shao, M. pH-dependent hydrogen and water binding energies on platinum surfaces as directly probed through surface-enhanced infrared absorption spectroscopy. *J. Am. Chem. Soc.* **142**, 8748–8754 (2020).
19. Wang, Y. H. et al. Spectroscopic verification of adsorbed hydroxy intermediates in the bifunctional mechanism of the hydrogen oxidation reaction. *Angew. Chem. Int. Ed.* **133**, 5772–5775 (2021).
20. Strmcnik, D. et al. Improving the hydrogen oxidation reaction rate by promotion of hydroxyl adsorption. *Nat. Chem.* **5**, 300–306 (2013).
21. Danilovic, N. et al. Enhancing the alkaline hydrogen evolution reaction activity through the bifunctionality of Ni(OH)$_2$/metal catalysts. *Angew. Chem. Int. Ed.* **124**, 12663–12666 (2012).
22. Subbaraman, R. et al. Trends in activity for the water electrolyser reactions on 3d M (Ni, Co, Fe, Mn) hydr(oxy)oxide catalysts. *Nat. Mater.* **11**, 550–557 (2012).
23. Dinh, C. T. et al. Multi-site electrocatalysts for hydrogen evolution in neutral media by destabilization of water molecules. *Nat. Energy* **4**, 107–114 (2019).
24. Men, Y., Li, P., Zhou, J., Chen, S. & Luo, W. Trends in alkaline hydrogen evolution activity on cobalt phosphide electrocatalysts doped with transition metals. *Cell Rep. Phys. Sci.* **1**, 100136 (2020).
25. Wang, Y. et al. Pt–Ru catalyzed hydrogen oxidation in alkaline media: oxophilic effect or electronic effect? *Energy Environ. Sci.* **8**, 177–181 (2015).
26. Intikhab, S., Snyder, J. D. & Tang, M. H. Adsorbed hydroxide does not participate in the Volmer step of alkaline hydrogen electrocatalysis. *ACS Catal.* **7**, 8314–8319 (2017).
27. McCrum, I. T. & Koper, M. T. The role of adsorbed hydroxide in hydrogen evolution reaction kinetics on modified platinum. *Nat. Energy* **5**, 891–899 (2020).
28. Li, J. et al. Experimental proof of the bifunctional mechanism for the hydrogen oxidation in alkaline media. *Angew. Chem. Int. Ed.* **56**, 15594–15598 (2017).

29. Rebollar, L. et al. "Beyond adsorption" descriptors in hydrogen electrocatalysis. *ACS Catal.* **10**, 14747–14762 (2020).

30. Ramaswamy, N. et al. Hydrogen oxidation reaction in alkaline media: relationship between electrocatalysis and electrochemical double-layer structure. *Nano Energy* **41**, 765–771 (2017).

31. Shen, L. F. et al. Interfacial structure of water as a new descriptor of the hydrogen evolution reaction. *Angew. Chem. Int. Ed.* **132**, 22583–22588 (2020).

32. Serva, A., Salanne, M., Havenith, M. & Pezzotti, S. Size dependence of hydrophobic hydration at electrified gold/water interfaces. *Proc. Natl Acad. Sci. USA* **118**, e2023867118 (2021).

33. Serva, A., Havenith, M. & Pezzotti, S. The role of hydrophobic hydration in the free energy of chemical reactions at the gold/ water interface: size and position effects. *J. Chem. Phys.* **155**, 204706 (2021).

34. Rosen, B. A. et al. Ionic liquid-mediated selective conversion of CO_2 to CO at low overpotentials. *Science* **334**, 643–644 (2011).

35. Hpone Myint, K., Ding, W. & Willard, A. P. The influence of spectator cations on solvent reorganization energy is a short-range effect. *J. Phys. Chem. B* **125**, 1429–1438 (2021).

36. Wang, T. et al. Enhancing oxygen reduction electrocatalysis by tuning interfacial hydrogen bonds. *Nat. Catal.* **4**, 753–762 (2021).

37. Berg, N., Bergwinkl, S., Nuernberger, P., Horinek, D. & Gschwind, R. M. Extended hydrogen bond networks for effective proton-coupled electron transfer (PCET) reactions: the unexpected role of thiophenol and its acidic channel in photocatalytic hydroamidations. *J. Am. Chem. Soc.* **143**, 724–735 (2021).

38. Lan, Y. Q. et al. Implanting numerous hydrogen-bonding networks in Cu-porphyrin based nanosheet to boost CH_4 selectivity in neutral media CO_2 electroreduction. *Angew. Chem. Int. Ed.* **60**, 2–9 (2021).

39. Alfarano, S. R. et al. Stripping away ion hydration shells in electrical double-layer formation: water networks matter. *Proc. Natl Acad. Sci. USA* **118**, e2108568118 (2021).

40. Serva, A., Scalfi, L., Rotenberg, B. & Salanne, M. Effect of the metallicity on the capacitance of gold–aqueous sodium chloride interfaces. *J. Chem. Phys.* **155**, 044703 (2021).

41. Le, J. B., Fan, Q. Y., Li, J. Q. & Cheng, J. Molecular origin of negative component of Helmholtz capacitance at electrified Pt(111)/water interface. *Sci. Adv.* **6**, eabb1219 (2020).

42. Limmer, D. T., Willard, A. P., Madden, P. & Chandler, D. Hydration of metal surfaces can be dynamically heterogeneous and hydrophobic. *Proc. Natl Acad. Sci. USA* **110**, 4200–4205 (2013).

43. Liu, Y., Kawaguchi, T., Pierce, M. S., Komanicky, V. & You, H. Layering and ordering in electrochemical double layers. *J. Phys. Chem. Lett.* **9**, 1265–1271 (2018).

44. Strmcnik, D. et al. Effects of Li^+, K^+, and Ba^{2+} cations on the ORR at model and high surface area Pt and Au surfaces in alkaline solutions. *J. Phys. Chem. Lett.* **2**, 2733–2736 (2011).

45. Grosjean, B., Bocquet, M. L. & Vuilleumier, R. Versatile electrification of two-dimensional nanomaterials in water. *Nat. Commun.* **10**, 1656 (2019).

46. Dubouis, N. et al. The fate of water at the electrochemical interfaces: electrochemical behavior of free water versus coordinating water. *J. Phys. Chem. Lett.* **9**, 6683–6688 (2018).

47. Dunwell, M., Yan, Y. & Xu, B. A surface-enhanced infrared absorption spectroscopic study of pH dependent water adsorption on Au. *Surf. Sci.* **650**, 51–56 (2016).

48. Yamakata, A. & Osawa, M. Dynamics of double-layer restructuring on a platinum electrode covered by CO: laser-induced potential transient measurement. *J. Phys. Chem. C* **112**, 11427–11432 (2008).

49. Osawa, M., Tsushima, M., Mogami, H., Samjeske, G. & Yamakata, A. Structure of water at the electrified platinum–water interface:

50. Zhu, S. et al. The role of ruthenium in improving the kinetics of hydrogen oxidation and evolution reactions of platinum. *Nat. Catal.* **4**, 711–718 (2021).

51. Huang, B. et al. Cation- and pH-dependent hydrogen evolution and oxidation reaction kinetics. *JACS Au* **1**, 1674–1687 (2021).

52. Tong, Y., Lapointe, F., Thämer, M., Wolf, M. & Campen, R. K. Hydrophobic water probed experimentally at the gold electrode/ aqueous interface. *Angew. Chem. Int. Ed.* **56**, 4211–4214 (2017).

53. Lambert, D. K. Vibrational Stark effect of adsorbates at electrochemical interfaces. *Electrochim. Acta* **41**, 623–630 (1996).

54. Liu, E. et al. Unifying the hydrogen evolution and oxidation reactions kinetics in base by identifying the catalytic roles of hydroxyl-water-cation adducts. *J. Am. Chem. Soc.* **141**, 3232–3239 (2019).

55. Jia, Q., Liu, E., Jiao, L., Li, J. & Mukerjee, S. Current understandings of the sluggish kinetics of the hydrogen evolution and oxidation reactions in base. *Curr. Opin. Electrochem.* **12**, 209–217 (2018).

56. Strmcnik, D. et al. The role of non-covalent interactions in electrocatalytic fuel-cell reactions on platinum. *Nat. Chem.* **1**, 466–472 (2009).

57. Intikhab, S. et al. Caffeinated interfaces enhance alkaline hydrogen electrocatalysis. *ACS Catal.* **10**, 6798–6802 (2020).

58. Kresse, G. & Hafner, J. *Ab initio* molecular dynamics for liquid metals. *Phys. Rev. B* **47**, 558–561 (1993).

59. Kresse, G. & Furthmüller, J. Efficiency of ab-initio total energy calculations for metals and semiconductors using a plane-wave basis set. *Comput. Mater. Sci.* **6**, 15–50 (1996).

60. Perdew, J. P. et al. Atoms, molecules, solids, and surfaces: applications of the generalized gradient approximation for exchange and correlation. *Phys. Rev. B* **46**, 6671–6687 (1992).

61. Grimme, S., Antony, J., Ehrlich, S. & Krieg, H. A consistent and accurate *ab initio* parametrization of density functional dispersion correction (DFT-D) for the 94 elements H-Pu. *J. Chem. Phys.* **132**, 154104 (2010).

62. Plimpton, S. Fast parallel algorithms for short-range molecular dynamics. *J. Comput. Phys.* **117**, 1–19 (1995).

63. Aktulga, H. M., Fogarty, J. C., Pandit, S. A. & Grama, A. Y. Parallel reactive molecular dynamics: numerical methods and algorithmic techniques. *Parallel Comput.* **38**, 245–259 (2012).

64. Shin, Y. K., Gai, L., Raman, S. & Van Duin, A. C. Development of a ReaxFF reactive force field for the Pt–Ni alloy catalyst. *J. Phys. Chem. A* **120**, 8044–8055 (2016).

65. Mathew, K., Kolluru, V. C., Mula, S., Steinmann, S. N. & Hennig, R. G. Implicit self-consistent electrolyte model in plane-wave density-functional theory. *J. Chem. Phys.* **151**, 234101 (2019).

66. Trasatti, S. The absolute electrode potential: an explanatory note (recommendations 1986). *Pure Appl. Chem.* **58**, 955–966 (1986).

67. Li, P., Huang, J., Hu, Y. & Chen, S. Establishment of the potential of zero charge of metals in aqueous solutions: different faces of water revealed by ab initio molecular dynamics simulations. *J. Phys. Chem. C* **125**, 3972–3979 (2021).

68. Li, P., Liu, Y. & Chen, S. Microscopic EDL structures and charge–potential relation on stepped platinum surface: insights from the *ab initio* molecular dynamics simulations. *J. Chem. Phys.* **156**, 104701 (2022).

69. Le, J., Iannuzzi, M., Cuesta, A. & Cheng, J. Determining potentials of zero charge of metal electrodes versus the standard hydrogen electrode from density-functional-theory-based molecular dynamics. *Phys. Rev. Lett.* **119**, 016801 (2017).

70. Marković, N. M., Grgur, B. N. & Ross, P. N. Temperature-dependent hydrogen electrochemistry on platinum low-index single-crystal surfaces in acid solutions. *J. Phys. Chem. B* **101**, 5405–5413 (1997).

71. Oberhofer, H., Dellago, C. & Geissler, P. L. Biased sampling of nonequilibrium trajectories: can fast switching simulations

outperform conventional free energy calculation methods? *J. Phys. Chem. B* **109**, 6902–6915 (2005).

72. Chan, K. & Nørskov, J. K. Electrochemical barriers made simple. *J. Phys. Chem. Lett.* **6**, 2663–2668 (2015).

73. Chan, K. & Nørskov, J. K. Potential dependence of electrochemical barriers from ab initio calculations. *J. Phys. Chem. Lett.* **7**, 1686–1690 (2016).

74. Yan, Y. G. et al. Ubiquitous strategy for probing ATR surface-enhanced infrared absorption at platinum group metal-electrolyte interfaces. *J. Phys. Chem. B* **109**, 7900–7906 (2005).

75. Liu, E. et al. Interfacial water shuffling the intermediates of hydrogen oxidation and evolution reactions in aqueous media. *Energy Environ. Sci.* **13**, 3064–3074 (2020).

Author contributions

S.C. supervised the project. P.L. and S.C. conceived the idea and designed the experiments. P.L. performed the AIMD simulations. Y.J. performed the electrochemical and spectroscopic measurements under the guidance of S.C. and W.C.; P.L., Y.J., Y.H., Y.M., Y.L and S.C. analysed the data. P.L., Y.J. and S.C. wrote the manuscript. All authors discussed and commented on the manuscript.

Competing interests

The authors declare no competing interests.

Additional information

Supplementary information The online version contains supplementary material available at https://doi.org/10.1038/s41929-022-00846-8.

Correspondence and requests for materials should be addressed to Shengli Chen.

Peer review information *Nature Catalysis* thanks Qingying Jia, Jun Cheng and the other, anonymous, reviewer(s) for their contribution to the peer review of this work.

Reprints and permissions information is available at www.nature.com/reprints.

Publisher's note Springer Nature remains neutral with regard to jurisdictional claims in published maps and institutional affiliations.